AIAA JOURNAL
Vol. 48, No. 2, February 2010

Characterization of a High-Frequency Pulsed-Plasma Jet Actuator for Supersonic Flow Control

Venkateswaran Narayanaswamy,* Laxminarayan L. Raja,† and Noel T. Clemens‡
University of Texas at Austin, Austin, Texas 78712

DOI: 10.2514/1.41352

An experimental study is conducted to characterize the performance of a pulsed-plasma jet (called a "spark jet" by other researchers) for potential use in supersonic flow control applications. A pulsed-plasma jet is a high-speed synthetic jet that is generated by striking an electrical discharge in a small cavity. The gas in the cavity pressurizes owing to the heating and is allowed to escape through a small orifice. To obtain an estimate of the relative strength of the pulsed-plasma jet, the jet is injected normally into a Mach 3 crossflow and the penetration distance is measured by using schlieren imaging. These measurements show that the jet penetrates 1.5 boundary-layer thicknesses into the crossflow and the jet-to-crossflow momentum flux ratio is estimated to be 0.6. A series of experiments was conducted to determine the characteristics of the pulsed-plasma jet issuing into stagnant air at a pressure of 35 torr. These results show that typical jet velocities of about 250 m/s can be induced with discharge energies of about 30 mJ per jet. Furthermore, the maximum pulsing frequency was found to be about 5 kHz, because above this frequency the jet begins to misfire. The misfiring appears to be due to the finite time it takes for the cavity to be recharged with ambient air between discharge pulses. The velocity at the exit of the jet is found to be primarily dependent on the discharge current and independent of other discharge parameters such as cavity volume and orifice diameter. Temperature measurements are made using optical emission spectroscopy and reveal the presence of considerable nonequilibrium between rotational and vibrational modes. The gas heating efficiency was found to be 10% and this parameter is shown to have a direct effect on the plasma jet velocity. These results indicate that the pulsed-plasma jet creates a sufficiently strong flow perturbation that holds great promise as a supersonic flow actuator.

Nomenclature

ρ_j = density of the pulsed-plasma jet
ρ_∞ = freestream density
u_j = exit velocity of the pulsed-plasma jet
u_∞ = freestream velocity

I. Introduction

DEVELOPMENT of surface plasma actuators for flow control applications has received considerable attention in recent years. The plasma actuators that have been developed to date rely on electrohydrodynamic (EHD) forces, electrothermal heating, and MHD forces (in the presence of imposed magnetic fields) as the principal flow actuation mechanisms. EHD forcing, in the form of dielectric barrier discharges (DBDs), has been the most extensively used for low-speed flow control applications [1]. DBD plasma actuators have been successfully used for separation control on flat plates [2,3], bluff bodies [4,5], and airfoils [6,7] and to induce mixing enhancement of jets [8]. The most common mechanism of plasma flow actuation for supersonic flow control has been the electrothermal heating produced using steady or pulsed glow and arc discharges. Because dc glow discharges have a relatively low power requirement per electrode, they therefore offer the potential for scalability over large surface areas. Kimmel et al. [9] have shown that a diffuse dc glow discharge with an input power of about 50 W could increase the surface pressure in the immediate vicinity of the cathode by about 10%. Owing to the instabilities in the discharge at high currents and pressure, it was concluded [10–12] that the effectiveness of a dc glow discharge is limited to currents of a few hundreds of milliamps. Leonov et al. [13] reported global changes were induced in a Mach 1.7 separated boundary layer by using a quasi-dc filamentary arc discharge. The limitation of using dc arc discharges has been the very high input power needed to cause significant heating. The limitation on high input power is overcome by Samimy et al. [14,15], who used a pulsed dc arc discharge to control the mixing of sub- and supersonic jets by perturbing the instability modes. In other recent work [16], a Lorentz force has been successfully applied to modify the position of the impinging shock foot location depending on the direction of the force. It should be noted that even though electrothermal heating and the Lorentz force have seen the most use in supersonic flow control, recent experiments have successfully employed DBDs to control the wake of a cylinder placed in a Mach 1.4 supersonic flow [17], and to excite boundary-layer instabilities in a supersonic boundary layer (e.g., [17,18]).

In this paper we investigate the use of a "pulsed-plasma jet" actuator for supersonic flow control. This actuator is essentially the same as the "spark jets" developed by Cybyk et al. [19,20]. In this type of actuator a discharge is struck inside a small cavity, which in turn electrothermally heats the gas inside the cavity. The pressurized gas is allowed to escape through a small hole in the cavity, which forms the pulsed-plasma jet. The pulsed-plasma jet has the distinct advantage in high-speed flows that it can generate high velocities with relatively modest power consumption. For example, computational simulations [19] have shown that a jet velocity as high as several hundred meters per second can potentially be achieved, and preliminary experimental results [20] have also shown that the velocity several diameters away from the jet exit is as high as 100 m/s. Another advantage of pulsed-plasma jets is that the jet momentum can be directed by changing the angle at which the jet issues into the flow. We note that a similar design, albeit at a much higher electrical power, was also used in "plasma igniters" developed for use in ignition of internal combustion engines [21]. The exit velocity of the gas from these plasma igniters is experimentally found to be about 500–1000 m/s for an energy input of about 1 J [22].

The objective of the current paper is to characterize the performance of the pulsed-plasma jet to establish its suitability as a supersonic flow control actuator. Toward this end we assess the

Received 6 October 2008; accepted for publication 29 September 2009.

*Graduate Research Assistant, Center for Aeromechanics Research, Department of Aerospace Engineering and Engineering Mechanics. Student Member AIAA.

†Associate Professor, Center for Aeromechanics Research, Department of Aerospace Engineering and Engineering Mechanics. Member AIAA.

‡Professor, Center for Aeromechanics Research, Department of Aerospace Engineering and Engineering Mechanics. Associate Fellow AIAA.

momentum of the pulsed-plasma jet by studying its penetration into a Mach 3 crossflow. We then characterize the flow and discharge properties of the pulsed-plasma jet actuator. The characterization included current/voltage measurements, optical emission spectroscopy, and time-resolved schlieren imaging. Optical emission spectroscopy was used to make temperature measurements to determine the gas heating efficiency of the discharge.

II. Principle of Operation

The pulsed-plasma jet operates by striking a short-duration, high-current electric arc in a closed cavity containing a small orifice [19]. The gas inside the cavity is electrothermally heated by the discharge, which leads to a rapid increase in pressure within the cavity. This high-pressure gas issues through the orifice and forms the pulsed-plasma jet. The velocity of the plasma jet is related to the cavity pressure, which in turn depends on the rate of deposition of energy. Inside the cavity the compression process that drives the jet is followed by a rarefaction wave that draws fluid back into the cavity and, hence, recharges it for the next pulse. Because the actuator operates without an external gas supply, the pulsed-plasma jet is a synthetic jet, which has zero net mass flux across the orifice.

III. Experimental Setup

A. Pulsed-Plasma Jet Actuator

The schematic and circuitry of a single pulsed-plasma jet actuator are shown in Fig. 1. This design is a modification of the design used in [19]. A cylindrical cavity of 2.4 mm diameter was made in ceramic (Macor^{TM}) plate and electrodes (2.4 mm diameter) were inserted from opposing sides to form a cavity bounded by electrodes. The gap between electrodes could be varied between 5 mm and 1.1 cm (0.2–0.4 in.) to provide different cavity volumes. A small hole, of 1.8 mm diameter, was drilled in the middle of cavity. Unless otherwise noted, the separation between the electrodes was fixed at 5 mm and the orifice diameter was set at 1.8 mm. Note that both the electrode spacing and the orifice diameter were varied in studies that specifically looked at the effect of varying these parameters on the jet velocity. The tip of the cathode was sharpened to decrease the breakdown voltage. A capacitor (0.22 μF) was charged by the dc power supply (Spellman, SL2PN1200) until the discharge was formed between the electrodes. Upon breakdown, the capacitor provided the high current required to sustain a nonequilibrium arc between the electrodes. A timing circuit, which included digital delay generators (Berkeley Nucleonics model 500B) and power MOSFET switches (STMicroelectronics model STP4N150), was made to repeat the charge–discharge cycle at kilohertz rates. Peak discharge currents (discharge set-point currents) ranging from 1.2 to 11 A were tested. A typical pulse width for the experiments was 20 μs, and above this value the jet velocity was independent of the pulse width. Pulsing frequencies up to 5 kHz were achieved at 2 A discharge current per cavity. Phase-locked schlieren imaging was performed to capture the instantaneous plasma jet structure at various time delays after the initiation of the discharge.

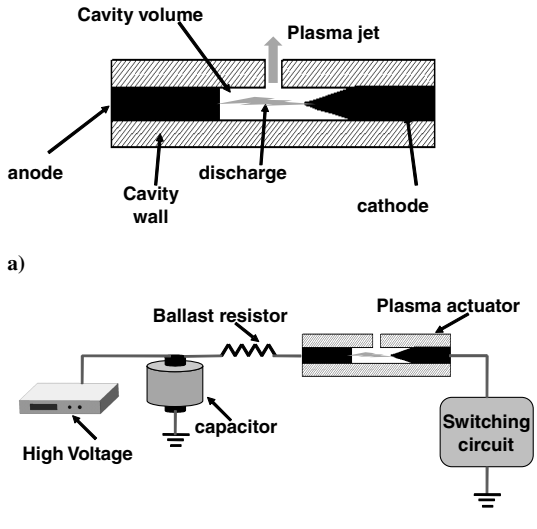

Fig. 1 Pulsed-plasma jet actuator: a) schematic, and b) circuitry.

B. Wind-Tunnel Facility

The experimental work to study the penetration of the pulsed-plasma jet into an incoming supersonic flow was conducted in a Mach 3 wind tunnel located at the University of Texas at Austin. The wind-tunnel test section has a cross-sectional area of 5×5 cm^2 and a length of 0.4 m. An acrylic splitter plate extends from the plenum section into the test section. The plasma actuator is placed at the trailing edge of the splitter plate. Pressurized air from a 500 ft^3 high-pressure tank is fed to the tunnel and is discharged into a 1000 ft^3 vacuum tank. The test section static pressure is maintained at 35 torr for all the cases studied. The incoming boundary layer is tripped several centimeters upstream of the jet orifice so as to obtain a fully developed turbulent boundary layer. The boundary layer-thickness of this tunnel, measured by previous workers [23], is approximately 4 mm.

C. Phase-Locked Schlieren Imaging

Phase-locked flash-lamp schlieren imaging was used to measure the contact-surface velocity and precursor shock velocity of the pulsed-plasma jet for the case of normal injection only (i.e., not pitched and skewed). The flash lamp was pulsed at 60 Hz using a digital delay generator (Berkeley Nucleonics model 500B), and the pulse duration of about 2 μs was small enough to provide an instantaneous snapshot of the flow. The flow was imaged through acrylic windows on each side of the test section. The light was collimated and focused by 1 m focal length concave mirrors. The schlieren images were captured using a complementary metal oxide semiconductor camera (Photron APX) operated with a framing rate of 60 Hz, triggered internally, and an exposure time of 16 ms. The images (1024×512 pixel resolution) were acquired for 10 s. Phase locking was achieved by pulsing the lamp at a predetermined delay from the start of the discharge trigger.

D. Spectroscopy

Optical emission spectroscopy was used to obtain temperature information from the plasma discharge. These measurements were performed for normal jet cases only. The light emitted from the discharge was collected with a 62.5 mm focal length confocal lens (50 mm diameter) through a glass side window and was focused on to a fiber optic cable with a 400 μm core. The orientation of the lens was such that it imaged directly into the cavity, that is, along the jet axis. The fiber optic was connected to the entrance slit (5 μm slit width) of a 1/4 m imaging spectrometer (Spectra-Physics MS260i). The nominal spectral resolution of the setup was 0.13 nm with an 1800 lines/mm grating. A study was performed to measure the spatial resolution of the optical setup by scanning a 25 μm pin hole across the object plane. The spatial resolution was limited by the fiber optic cable core diameter and the magnification of the system and was approximately 400 μm.

IV. Results

A. Assessment of the Strength of the Pulsed-Plasma Jet

Initial tests were performed to assess the strength (i.e., induced momentum) of the pulsed-plasma jet. This was accomplished by studying the penetration of the pulsed-plasma jet injected normally to the incoming Mach 3 flow. For these studies the penetration was measured from schlieren images that were acquired at various delay times from the start of the discharge trigger signal. The discharge was pulsed at 60 Hz and the schlieren was acquired at the same rate. At least 50 images were averaged at each time delay to render the phase-average image corresponding to the time delay. The peak discharge

current of the pulsed-plasma jet was 1.2 A and a single jet was injected into the flow. The flowfield without pulsed jet injection is shown in Fig. 2a. The Mach waves seen as bright and dark lines crisscrossing the image are due to imperfections in the ceiling and floor walls and they do not affect the flow. Also, it should be noted that the jet exit hole itself does not create any noticeable Mach wave or shock. A schlieren image of the pulsed-plasma jet issuing into the Mach 3 crossflow is shown in Fig. 2b for a time delay of 35 μs after the start of the discharge trigger. This time delay corresponds to the maximum penetration of the jet. The injection port is located roughly in the middle of the frame as indicated. The shock (labeled shock due to plasma jet) upstream of the jet marks very closely the upstream boundary of the jet. The jet itself is seen as a relatively bright region in the figure (labeled plasma jet). Given the knife-edge position used, the relatively brighter appearance of the jet indicates that it has a lower density (i.e., is hotter) than the surrounding fluid. The penetration of the jet is measured "by eye" by estimating the distance of the approximate jet centerline at its maximum penetration from the floor, as shown in Fig. 2b. From Fig. 2b the transverse penetration length of the jet is approximately 1.5δ or three orifice diameters. From previous studies on the penetration of steady jets in crossflow [24], and accounting for the previous observation that pulsing increases the penetration by 12% [25], the momentum flux ratio $(\rho_j u_j^2/\rho_\infty u_\infty^2)$ of the pulsed-plasma jet compared to the freestream is about 0.6. This momentum flux ratio shows that the pulsed-plasma jet momentum flux is of the same order of magnitude as that of the supersonic crossflow.

B. Pulsed-Plasma Jet Issuing into Stagnant Air

The preceding section shows that pulsed-plasma jets hold promise as high-bandwidth actuators for controlling high-speed flows. With this as motivation, a detailed study was conducted to characterize the discharge and velocity of the plasma jet. For these studies the jet issued into a vacuum chamber filled with stagnant air at a pressure of about 35 torr. The measurements made include the jet contact-surface velocity, rotational and vibrational temperatures of the discharge, and voltage-current characteristics of the plasma jet. The 35 torr pressure was used because it is approximately the same as the static pressure of the Mach 3 wind-tunnel freestream. The pulse width of the discharge was 20 μs unless stated otherwise. The pulsing frequency of the discharge was 60 Hz. We note that as long as the pulsing frequency remains less than a few kilohertz then the frequency does not significantly affect the parameters of interest in this study. This frequency dependence will be discussed in Sec. IV.B.4.

The results are organized in the following manner. The current-voltage characteristic of the discharge is discussed first. These measurements clarify the nature of the discharge. This section is followed by the contact-surface velocity measurement performed at several different conditions. The various parameters that influence the plasma jet velocity are explored. This is followed by rotational and vibrational temperature measurements using optical emission spectroscopy.

1. *Current-Voltage Characteristics*

Typical time histories of anode voltage and discharge current during a pulse are shown in Fig. 3. The pulsing frequency of the discharge was 60 Hz. The anode voltage was measured using a high-voltage probe with gigahertz bandwidth (Tektronics P6015A), and the discharge current was inferred from the voltage drop across a 1.2 Ω resistor placed downstream of the cathode. The measurement uncertainty of the high-voltage probe quoted by the manufacturer is $\leq 3\%$. Once the discharge was initiated, the anode voltage decreased from 2 kV to about 0.8 kV in less than 5 μs and then decreased to about 300 V after 40 μs. The discharge current reached the set-point value ($\approx$1.7 A in Fig. 3) in about 5 μs. The discharge current density, based on the electrode cross-sectional area, is estimated to be about 10^5 mA/cm^2. Based on this current density we infer that the discharge is essentially a highly constricted arc with possibly a high degree of nonequilibrium associated with the large gradients due to the small discharge volume [26]. From the V–I plot shown, the input power into the discharge is estimated to be about 1 kW and the total energy input during the 20 μs time period is about 20 mJ. The current-voltage trace is found to be the same for all the discharge currents tested in this study.

It should be noted that only square-wave discharge pulses were used to ensure that the energy was deposited at a high rate. The rate of deposition of energy depends on the slope of the discharge current, which is maximum for a square waveform. Also it was demonstrated that the maximum exit velocity of the jet does not depend on the pulse width for pulse widths larger than 20 μs.

2. *Flow Structure Around the Plasma Jet*

The flow structure of the plasma jet was observed by using phase-locked schlieren imaging at various delay times from the start of the discharge trigger. Figure 4 shows the typical flow structure for a time delay of 30 μs. The plasma jet is seen to develop as a typical mushroom-shaped structure. A spherically symmetric precursor shock produced by the impulsively started jet is also seen above the jet contact surface. The absence of a Mach disk within the jet indicates that the local Mach number of the jet is subsonic. It should be emphasized that more than three runs were made for a given discharge current and time delay to test the repeatability of the contact

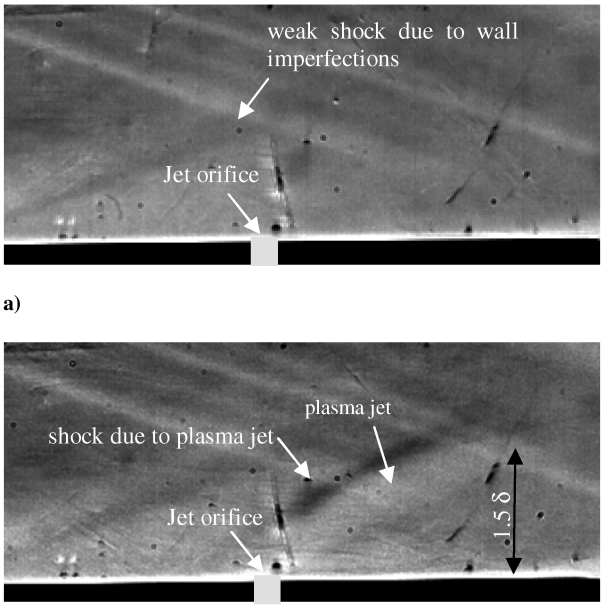

Fig. 2 Phase-average schlieren images showing the penetration of normally injected pulsed-plasma jet: a) flowfield without the jet, and b) phase averaged image 35 μs after the start of discharge trigger.

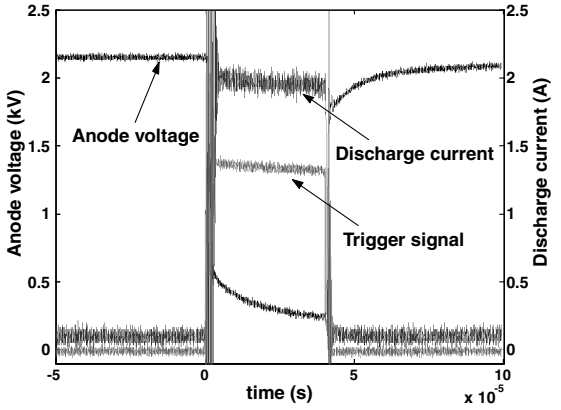

Fig. 3 Typical current-voltage characteristic of one pulse of the pulsed-plasma discharge. The pulsing frequency of the discharge was 60 Hz.

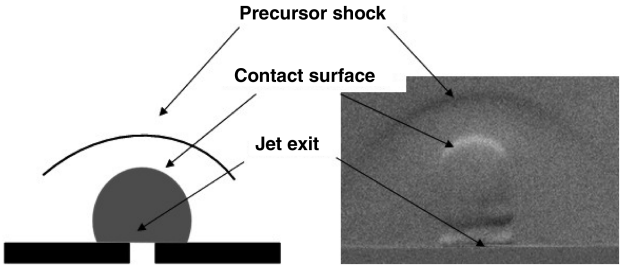

Fig. 4 Flow structure of one of the jet pulses. The pulsed-plasma discharge set-point current is 3.9 A. The image shown is taken 30 μs after the start of discharge trigger.

surface and precursor shock trajectories. The standard deviation of the contact-surface trajectory at different time delays estimated from phase-locked imaging was found to be less than about 10% (see Fig. 6) for a 1.2 A plasma jet.

3. *Contact-Surface Trajectory*

A phase-averaged schlieren time sequence was generated by capturing approximately 100 images at several delay times. For each time the locations of the phase-averaged contact surface and precursor shock (with respect to the jet exit) were measured. The resulting trajectories of these flow features are shown in Fig. 5. For this figure the peak discharge (set-point) current was 3.9 A. Figure 5 shows that the trajectory of the precursor shock is linear over the entire time period, which indicates its velocity is constant over the range of times considered. In contrast, the contact surface slows down with increasing distance from the orifice. Figure 6 shows a comparison of the contact-surface trajectories at the two discharge set-point currents of 1.2 and 3.9 A. For the 1.2 A case, the contact surface first becomes visible 15 μs from the start of the discharge trigger, whereas for the 3.9 A case, it takes only 10 μs. Also, the slopes of the trajectories indicate that the 1.2 A discharge generates a lower-velocity jet as compared to the 3.9 A discharge. This is expected because the higher discharge current causes more rapid heating and, hence, a higher rate of pressurization in the discharge cavity than the lower discharge currents. The short time delay between the discharge trigger and the appearance of the jet indicates that the jet responds very rapidly. However, the bandwidth of the actuator is determined by the startup transient as well as the time required to refill the cavity with gas. This will be discussed further in Sec. IV.B.4.

4. *Jet Velocity Measurements*

The contact-surface velocity was measured from the slope of the contact-surface trajectory close to the jet exit. It must be noted that the contact-surface velocity is not necessarily the same as the local jet fluid velocity because the jet velocity can be influenced by trailing

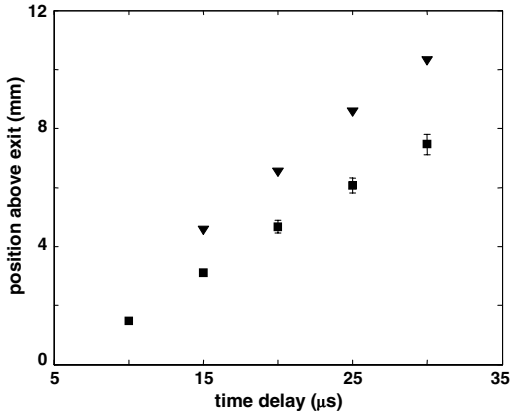

Fig. 5 Trajectory of the pulsed-plasma jet precursor shock (triangles) and contact surface (squares) for a discharge set-point current of 3.9 A. Time delays are measured from the start of the discharge trigger. Position of the contact surface is measured from the jet exit.

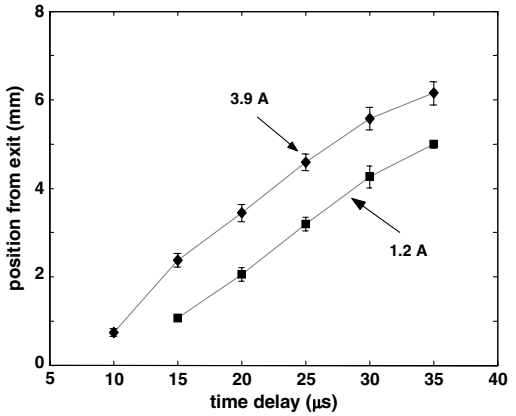

Fig. 6 Comparison of trajectories of the contact surface of the pulsed-plasma jet for two discharge set-point currents of 1.2 and 3.9 A. Time is measured from the start of the discharge trigger. Position of the contact surface is measured from the jet exit.

expansion waves. As a consequence, we expect the contact-surface velocity to give an upper limit to the local jet fluid velocity. With this caveat in mind, the following discussion will refer to the measured contact-surface velocity as the jet velocity.

A survey was made of the factors that influence the strength of the jet as quantified by the jet velocity close to the jet exit. One of the main factors that affects the jet velocity is the discharge current because it dictates the input energy. Figure 7 shows the variation of the jet velocity with discharge current. In all cases the separation between the electrodes was 0.5 cm and the orifice diameter was 1.8 mm. The velocity increases from about 230 m/s at a 1.2 A set-point current to about 320 m/s at 12 A. Thus, there is just a 30% increase in velocity for a tenfold increase in discharge current. We discuss this issue further in the next section. We have also found that the strength of the jet depends on the material of the cavity. For example, the jet velocity increased by about 30% when boron nitride, which has a higher thermal conductivity and corrosion resistance, was used instead of Macor^{TM} ceramic. A possible explanation for this observation is given in Sec. IV.B.4. We also conducted a preliminary study of the effect of the geometric parameters on the exit velocity of the jet. The two parameters varied were the orifice diameter and the cavity volume. Orifice diameters were varied from 0.25 to 1.8 mm. The jet exit velocity variation with respect to the orifice diameter is shown in Fig. 8. It can be seen that the magnitude of the velocity is roughly the same for all the diameters tested. The effect of the cavity volume on the jet exit velocity was investigated for two volumes. The cavity volume was changed by changing the separation distance between the electrodes while leaving the cross-sectional area of the cavity the same. A 1 cm (0.4 in.) separation distance corresponded to a cavity volume of $\approx$0.04 cm^3, whereas a 0.5 cm

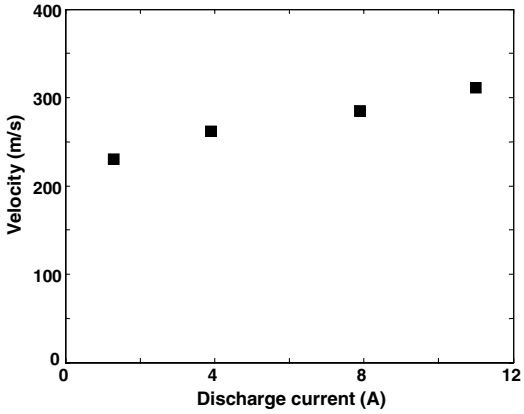

Fig. 7 Variation of the plasma jet velocity with increasing discharge set-point currents.

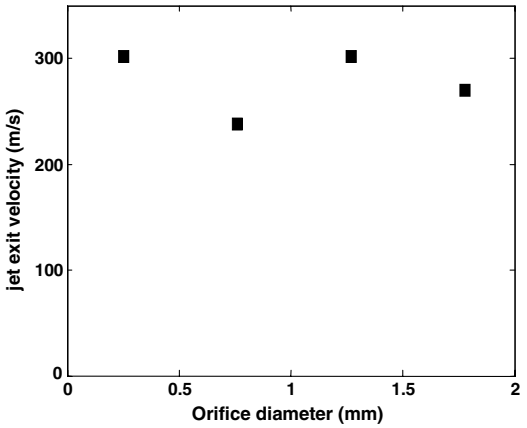

Fig. 8 Variation of jet exit velocity of the pulsed-plasma jet with respect to different orifice diameters. The discharge current is set at 3.9 A.

(0.2 in.) separation corresponded to a volume of ≈ 0.02 cm^3. It was found (figure not shown here) that the trajectories of the jet for the two cavity volumes were approximately the same, and the jet exit velocities were very similar in both cases. It can be concluded that the jet exit velocities are relatively insensitive to the particular choice of the jet exit diameter and cavity volume used in the current study.

Another important parameter of interest is the pulsing frequency. The pulsing frequency essentially determines the cavity recharge time available between pulses. Figure 9 shows a train of discharge current pulses for two frequencies: 5 and 10 kHz. Figure 9a corresponds to 5 kHz pulsing, whereas Figs. 9b and 9c correspond to two different experimental realizations at 10 kHz. At 5 kHz, a discharge pulse occurs reliably for every trigger signal. Also the discharge current remains unchanged during each pulse. In contrast, at 10 kHz (Figs. 9b and 9c) we observe somewhat erratic pulsing behavior wherein occasional pulses are missed in the pulse train. One can see also that occasionally the peak pulse current gradually decreases during a continuous pulse train until the pulse train completely pauses without any discharge activity for a few hundred microseconds before the pulse discharge activity resumes once again. The erratic pulsing at the higher frequency may be because of some inherent limitations in the electrical circuitry (such as the capacitance of the circuit, including the electrode gap) or due to the finite time for replenishment of the fluid in the cavity. Some experiments were conducted to test the limitations of the circuitry at a high frequency. First the cathode and anode were replaced with a resistor that was equivalent to that of the discharge. In this configuration, pulsing rates of over 100 kHz were obtained reliably. Then a pulsed dc discharge circuit was made, except the electrodes were exposed to the ambient pressure (35 torr) in a low-pressure chamber rather than being enclosed in a cavity. This test takes into account the limitations inherent to the circuitry and also the capacitance of the electrode gap. The circuit was able to maintain repeatable pulsing to frequencies as high as 20 kHz without loss of current. Moreover, from Fig. 3 it can be seen that the anode voltage recovers to its original value before the plasma was switched on (≈ 2.1 kV) in less than 60 μs. These observations lead us to conclude that this pause of a few 100 μs in the discharge activity is a consequence of the cavity replenishment timescale being longer than the interpulse period. Given that the pulsing occurs reliably up till 5 kHz, one can infer that the minimum replenishment time needed for producing next reproducible pulse for a 1.2 A pulsed-plasma jet is about 200 μs.

A comparison of the jet velocities at the two frequencies of 60 Hz and 5 kHz was also made for a 1.2 A discharge. It was found that the velocities were identical, to within the experimental uncertainty, which indicates the jet velocity is independent of pulsing frequency for frequencies up to 5 kHz. However, the anode-voltage trace at these two different frequencies shows that, for a fixed set-point current of 1.2 A, the anode voltage during the discharge pulse was about 1.4 kV for a 5 kHz discharge and 400 V for a 60 Hz discharge (the waveforms are not shown here). At the higher pulsing frequency

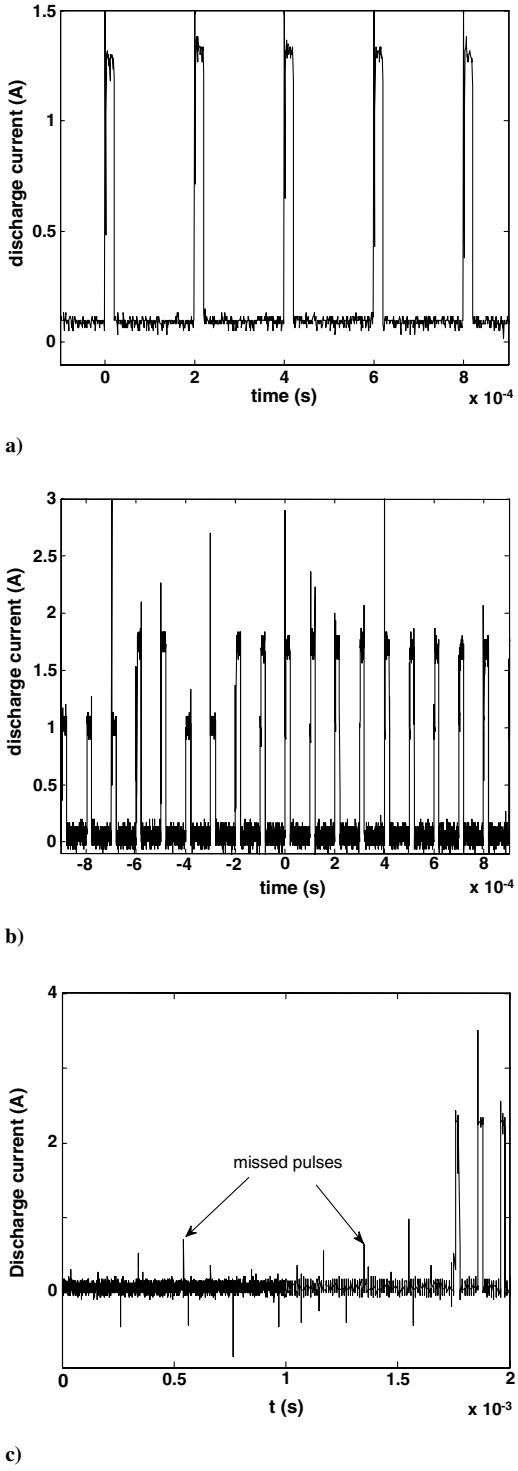

Fig. 9 Discharge current pulse transients at different pulsing frequencies for a 1.2 A discharge set-point current: a) pulsing frequency of 5 kHz, b) pulsing frequency of 10 kHz showing pulse-to-pulse variation in discharge current, and c) pulsing frequency of 10 kHz showing missing pulses during a sequence.

the discharge is likely to have a higher degree of nonequilibrium, whereas at the lower frequency it is likely to exhibit a more equilibrium arclike discharge, because arc discharges are characterized by lower discharge voltage compared to nonequilibrium glowlike discharges. The following is a plausible explanation for the observed transition from an arclike discharge at low pulsing frequency (60 Hz) to a glowlike discharge at a high pulsing frequency (5 kHz). At the end of each pulse the gas in the cavity is left hot and it takes a finite time for it cool down. When the pulses are in quick succession the gas in the cavity has a shorter amount of time to cool down before the next

pulse. Hence, the average cavity temperature of a higher-frequency pulsed-plasma jet should be higher than for a lower-frequency case. A consequence of the higher temperature is that the density of the gas inside the cavity for a 5 kHz discharge is significantly lower than that for a 60 Hz discharge, which causes a higher reduced electric field E/N (where E is the electric field and N is the background gas number density) in the discharge, resulting in a higher degree of nonequilibrium. However, at elevated currents (>2 A) the discharge is arclike even at kilohertz pulsing rates as evident from the lower anode voltages during the pulse for the higher pulsing frequencies. The independence of jet velocity with respect to pulsing frequency also implies that the jet velocity does not depend on the nature of the discharge for a fixed discharge current.

It is worth noting that this discussion is also consistent with our observation that a boron–nitride cavity resulted in a higher pulsed-plasma jet velocity than a Macor™ cavity. Boron nitride has higher thermal conductivity than Macor™, and so it is likely that the boron–nitride cavity remained cooler than the Macor™ cavity and, hence, maintained a higher density. As argued earlier, the higher gas density leads to less nonequilibrium and, hence, more gas heating.

5. *Nonequilibrium Effects in the Discharge*

To obtain more quantitative estimates of the degree of nonequilibrium, measurements of the N_2 rotational and vibrational temperature were made at different discharge currents, pulsing frequencies, and pulse widths. The rovibronic emission spectrum of N_2 in the wavelength range from 365 to 395 nm was measured with a spectrograph. The N_2 second positive system ($C_u^3\Pi_u \rightarrow B^3\Pi_g$) with bandheads at 380.49 nm (0–2 vibrational transition), 375.54 nm (1–3), and 371.05 nm (2–4) was observed. The rotational temperature was found by fitting the observed rotational spectra with synthetic spectra corresponding to different rotational temperatures. The vibrational temperature was found by matching the bandhead intensities for different vibrational transitions. The procedure is described in detail in Shin et al. [27]. The resulting uncertainty in rotational temperature due to the difference in the measured spectrum and synthetic spectrum fit is estimated to be about 10–15%. Figure 10 shows a typical spectrum obtained for a 6.5 A discharge with a 20 μs duration. The rotational temperature is about 800 K and the vibrational temperature is about 3100 K. In comparison, for a 1.2 A discharge the rotational temperature is about 600–700 K and the vibrational temperature is about 2800 K. Thus, the pulsed discharge is characterized by a high degree of thermal and chemical nonequilibrium through the entire range of discharge currents employed in this work. Note that the measured temperatures are significantly lower than those reported in [28] for a nonenclosed pulsed arc at 1 atm. They reported a rotational temperature of about 2000 K for a 250 mA discharge with a 20 μs pulse width. This temperature is considerably closer to the equilibrium temperature, which is not surprising considering the higher pressure of the discharge.

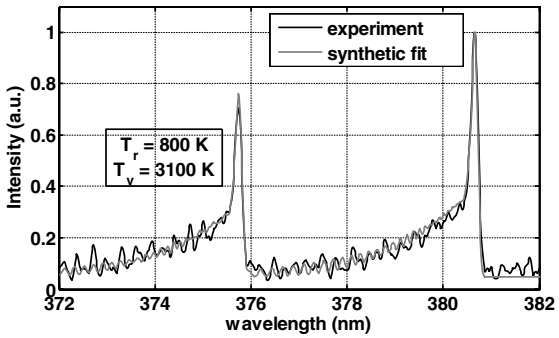

Fig. 10 Measured (black curve) and synthetic fit (gray curve) of the optical emission spectrum obtained from the 6.5 A pulsed-plasma discharge. The rotational temperature (T_r) for the best fit is 800 K and the vibrational temperature (T_v) is 3100 K. The uncertainty in the temperature estimate (see [27]) is about 10–15%.

The nonequilibrium distribution can be explained considering the different molecular collisional/relaxation processes involved in gas heating in an electric discharge. An illustration of the dominant energy pathways in the plasma is shown in Fig. 11. The input energy in the electric field is transferred most efficiently to the plasma electron pool via electron joule heating (energy in the electron being quantified by the electron temperature T_e). The imposed electric field also couples energy to the ion species via ion joule heating (quantified by a distinct ion temperature T_i). The thermal energy of the ions is, however, quickly equilibrated with the other neutral heavy species in the discharge owing to efficient collisional transfer resulting in $T_i \approx T_g$, a common heavy species (gas) temperature. The electron energy remains relatively decoupled from thermal energy of the heavy species (ions and neutrals) (i.e., $T_e > T_g$), owing to the large disparity in particle mass between electrons and other species [10]. The high kinetic energy of the electrons is lost via electron elastic collisions with the heavy species (an inefficient process, as mentioned earlier) and electron inelastic collisions (vibrational and electronic excitation) with the heavy species. In a molecular gas (such as air), inelastic vibrational excitation of N_2 and O_2 molecules is particularly efficient and can be the dominant pathway for electron energy loss. The vibrationally excited gas molecules can transfer

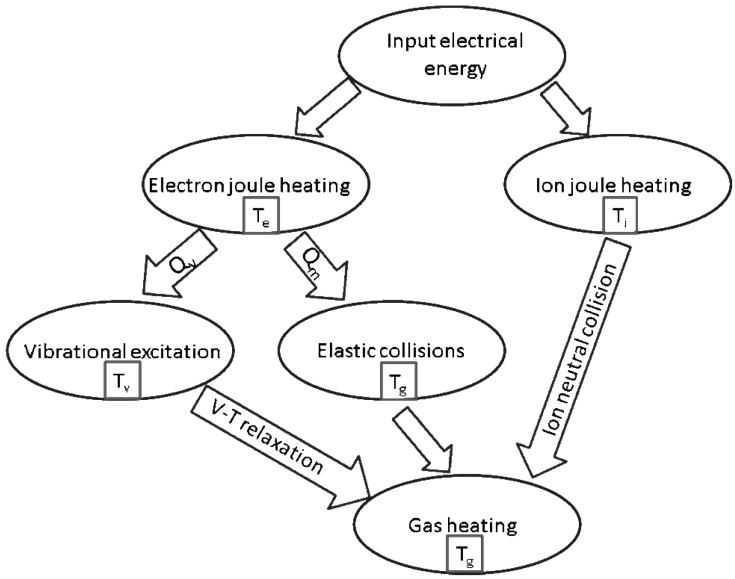

Fig. 11 Illustration of the important energy transfer pathways that contribute to gas heating the pulsed discharge.

their energy to thermal energy (causing gas heating) via vibrational–translational relaxation, which has a characteristic timescale of milliseconds for vibrationally excited N_2 and O_2 under the conditions of the discharge in this study [10,29]. Because the pulse width of the discharge is about 20 μs, the gas heating due to V-T relaxation during this time period is negligible, resulting in a decoupling of the vibrational energy of molecules from the thermal energy. In summary, a large part of the input electrical energy in the discharge can be trapped in the electron thermal energy and the molecular vibrational energies, which is detrimental to the operation of the pulsed-plasma discharge for flow actuation purposes.

The following estimates can be made for the conditions of the discharge in this study. From the discharge current density ($\sim$45 A/cm^2) and electric field of 400 V/cm (assuming a linear drop of electric potential between cathode and anode), the ion and electron (assuming a quasi-neutral discharge) number densities are estimated to be about 10^{13} cm^{-3}. This estimate was made by solving for the electron number density by using Ohm's law with a known current density and electric field. The unknown electron number density is implicit in the electric conductivity. The empirical relations and experimental data given in [10] were used. The estimated electron number density is several orders of magnitude smaller than the neutral number density ($\sim 10^{18}$ cm^{-3}). For the computed values of ion and electron number densities, and the applied electric field, the fraction of input electric energy that goes into ion joule heating is computed to be about 0.06%. It is thus evident that the contribution from ion neutral collisions toward gas heating is negligible. Hence, almost the entire input electrical energy is used for electron joule heating. The partition of electron joule heating into rotational and vibrational modes of neutrals can be estimated by comparing the cross sections for rotational and vibrational energy transfer. The cross sections of N_2 alone are considered for this analysis, which is justified because N_2 is the dominant species of the air plasma employed in this study. The numerical values of cross sections are obtained from [30–33]. For a pressure of 35 torr, the reduced electric field E/N is about 16 Td. It must be mentioned that the cross-sectional values do not change significantly for the E/N values in the range of 1–200 Td; hence, the error introduced by an inaccurate estimation of the electric field is quite small. From the theoretical computations based on cross section performed for N_2 at 77 K in [30], it is seen that about 90% of the input power goes into excitation of vibrational modes whereas less than 10% goes into rotational modes. Thus, almost the entire input energy is locked up in vibrational modes for which the relaxation time scale is orders of magnitude larger than the discharge time scale; hence, the vibrational temperature is expected to be much higher than the rotational temperature. However, at a high pressure ($\sim$1 atm) and for the same value of electric field, the E/N ratio would be about 50 times smaller. For such small values of E/N the fraction of input energy that goes into gas heating increases rapidly to about 90% [30], which is close to the value observed in [28]. A direct measurement of the fraction of input energy that goes into gas heating is performed in [34,35]. Gas heating of pulsed N_2 plasma at 300 K and at different E/N values was studied both theoretically and experimentally in [34]. Based on these results, we observe that only about 10% of input energy goes toward gas heating, whereas 90% goes into vibrational excitation. Similar heating efficiency is also reported by Smy et al. [35], who used a plasma jet facility with input energy of about 1 J at 0.1 atm pressure. Assuming that 10% of the input energy goes into gas heating as estimated from cross sections and heating efficiency given in [30], we calculate that gas temperature for a 1.2 A, 20 μs pulse width discharge should be about 600 K (compared to the measured value of 600–700 K), and that for 6.5 A discharge is about 1500 K (compared to the measured value of about 800–1000 K; see Figs. 10 and 12). Thus, the calculated values of temperature are within a factor of 2 of the measured temperature.

A theoretical estimate of the jet velocity can be obtained by a shock-tube problem analysis. This analysis was successfully employed in [21] to obtain the exit velocity from a plasma igniter. Considering the rapidity of the heating by electric discharge in the present application, we expect that the shock-tube analysis should yield a reasonable estimate of the jet exit velocity for the pulsed-plasma jet also. We adopt the nomenclature used in [36] for our analysis. The instantaneous energy deposition by the electric discharge (analogous to the rupture of diaphragm in a shock tube) creates a precursor shock that propagates into the ambient and a train of rarefaction waves that travel into the cavity (analogous to the driver section). The passage of rarefaction waves causes a decrease in pressure of the gas. Hence, there is a smooth decrease of pressure from its initial high value (defined here as P_4) at the head of the rarefaction wave to the station just behind the precursor shock (P_3). The latter can be calculated from the normal shock relations with the knowledge of the precursor shock propagation velocity obtained from the shock trajectory in Fig. 5. The initial high pressure P_4 is the cavity pressure at the end of energy deposition. Its value can be calculated from the ratio of gas temperature (T_g) obtained using spectroscopic measurements and ambient temperature, assuming constant volume heating. The exit velocity of the jet is assumed to be the same as the velocity of the downstream edge of the precursor shock. This assumption is reasonable because, close to the jet exit, the precursor shock and the contact surface are close to each other. The exit velocity is thus calculated using the relation

$$v_3 = a_4 \times [2/(\gamma - 1)] \times [1 - (p_3/p_4)^{\frac{\gamma-1}{\gamma}}] \qquad (1)$$

where a_4 is the speed of sound in the cavity (driver section) after energy deposition.

For $T_g = 700$ K (as in the case of a 1.2 A pulsed-plasma jet), the jet velocity is estimated from Eq. (1) to be about 370 m/s. Furthermore, for $T_g = 800$ K (Fig. 10), which was measured at a current of 6.5 A, Eq. (1) yields a jet velocity of about 400 m/s. However, the jet velocity obtained is about 230 m/s for a 1.2 A pulsed-plasma jet and 300 m/s for a 6.5 A pulsed-plasma jet. Though the theoretical velocities computed using the instantaneous heating model are of the same order of magnitude as the measured values, there is still a disparity of about 60%.

The disparity between the predicted and measured velocities is perhaps explained as a limitation of the instantaneous heating assumption. To explore this possibility an attempt was made to measure the temporal evolution of the discharge temperature during the discharge pulse. Because our spectrometer did not allow us to make gated measurements, an indirect estimate of the temporal evolution of the discharge temperature was made. As the intent was to demonstrate a gradual heating by the electric discharge, this approximate estimate was found to be adequate. It should be noted that we do not make any quantitative conclusions from this measurement. The discharge temperature was measured for a 6.5 A pulsed discharge with different pulse widths, viz., 10, 15, and 20 μs. The temperature measured at a given pulse width is assumed to be a representative weighted average of the temperature of the discharge during the

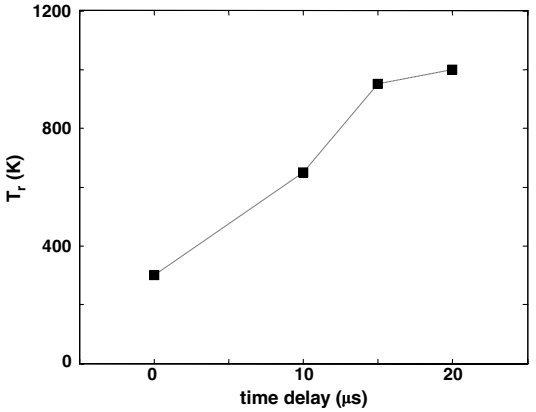

Fig. 12 Rotational temperature obtained for a 6.5 A pulsed-plasma jet with different pulse widths. The pulse width of 0 μs corresponds to the ambient temperature (no plasma). The variation of the rotational temperature with pulse width is an indication of the time evolution of the rotational temperature of the discharge.

discharge pulse. In other words, the temperature measurement of a 10 μs pulse width discharge would correspond to a weighted average discharge temperature between 0 and 10 μs. Similarly, a 15 μs pulse width discharge would correspond to a weighted average gas temperature between 0 and 15 μs, and so on. Also the temperature of the discharge at an instant within a given pulse width does not depend on the evolution of the discharge after that instant. That is to say, the temperature at the end of, say, 10 μs in a 20 μs discharge does not depend on the discharge temperature at a time later than 10 μs. Thus, the temperature at the end of 10 μs depends only on the discharge evolution between 0 and 10 μs and is independent of the discharge evolution at later times ($t > 10$ μs). By this reasoning, the gas temperature measurement at different discharge pulse widths would, in effect, give a pseudo time series of the temperature of the discharge during the evolution of the pulsed-plasma jet. Figure 12 shows the pseudo temporal evolution of the gas temperature of a 6.5 A pulsed discharge. The representative discharge temperature between 0 and 10 μs is plotted at 10 μs and the representative discharge temperature between 0 and 15 μs is plotted at 15 μs, and so on. It is clearly seen that the gas heating is not instantaneous and the time scale of gas heating is about 10 μs. This suggests a gradual heating of the cavity and, hence, may explain why the theoretical velocity estimate, which assumes instantaneous gas heating, overpredicted the jet velocity.

Finally, we define the efficiency of the pulsed-plasma jet as the ratio of the total kinetic energy (KE) issued from the cavity over a cycle to the input energy. The total kinetic energy is defined as

$$\mathrm{KE} = \int_0^\tau \frac{1}{2}\dot{m}u_j^2 \,\mathrm{d}t$$

where $\dot{m}$ is the jet mass flow rate and τ is the time period of the discharge. A typical case of a 6.5 A peak discharge current is considered for this analysis. The rotational temperature measured from spectroscopy for this case is about 800 K, which is taken as the gas temperature. By using this temperature and assuming a constant ratio of specific heats, we estimate the thermal energy deposited per cycle to be 1.2 mJ. A first-order model of the process was developed in [19] and this was used to estimate the mass expelled from the cavity. The model predicts that 20% of the mass in the cavity is expelled during each cycle, and we further assume that this mass is expelled at a uniform rate. Combining these values with the aforementioned velocity measurements, the efficiency of the pulsed-plasma jet actuator is about 4%. We note that a systematic study of the effect of gas temperature on the discharge current was not made, and so we cannot comment on the dependence of the efficiency on the input power; however, this is an important issue that will be explored in future work.

V. Conclusions

A pulsed-plasma actuator was studied in this work, which holds promise for supersonic flow control applications owing to its high bandwidth (~kHz) and high-injection velocity (~300 m/s). This actuator has the further advantage that the momentum that issues from the jet can be injected into the flow at directed angles. Initial tests to assess the strength of the pulsed-plasma jet showed that the jet injected normally into the supersonic crossflow penetrated (in the transverse direction) about 1.5δ. The estimated jet-to-crossflow momentum flux ratio was 0.6, which indicates the jet momentum flux is comparable to that of the supersonic freestream. It can be concluded from these measurements that the pulsed-plasma jet is a promising actuator for high-speed flow control applications.

A thorough characterization of a jet issuing into a static vacuum chamber was conducted. The jet velocity was shown to be a function of the discharge current and the cavity material and independent of other relevant factors studied. The jet velocity was of order 300 m/s and increased only by 30% (from 250 to 330 m/s) for a tenfold increase in discharge current (from 1.2 to 11 A). Reliable and repeatable pulses were obtained for frequencies up to about 5 kHz. Above 5 kHz the discharge would begin to miss pulses, which we believe is due to the finite gas recharge time of the cavity. Spectroscopic measurements suggested that the discharge was characterized by a high degree of thermal nonequilibrium. The fraction of power that goes to gas heating was estimated to be about 10% of the input power, which is consistent with the values available in the literature. This inefficient gas heating is believed to be the main reason for the low jet velocity compared to the theoretical estimate of about 1000 m/s made in [19,20]. The finite time for energy deposition was also indirectly determined by measuring the evolution of the local-average gas temperature for different duration pulses. These measurements were used to explain the effect of gradual gas heating on the jet exit velocity of the pulsed-plasma jet.

References

[1] Moreau, E., "Airflow Control by Non-Thermal Plasma Actuators," *Journal of Physics D: Applied Physics*, Vol. 40, 2007, pp. 605–636. doi:10.1088/0022-3727/40/3/S01

[2] Roth, J. R., Sherman, D. M., and Wilkinson, S. P., "Boundary Layer Flow Control with a One Atmosphere Uniform Glow Discharge Surface Plasma," AIAA Paper 98-0328, 1998.

[3] Jukes, T. N., Choi, K. S., Jonhson, G. A., and Scott, S. J., "Turbulent Boundary Layer Control for Drag Reduction Using Surface Plasma," AIAA Paper 2004-2216, 2004.

[4] Thomas, F. O., Kozlov, A., and Corke, T. C., "Plasma Actuators for Bluff Body Flow Control," AIAA Paper 2006-2845, 2006.

[5] McLaughlin, T. E., Munska, M. D., Vaeth, J. P., Dauwalter, T. E., Goode, J. R., and Siegel, S. G., "Plasma-Based Actuators for Cylinder Wake Vortex Control," AIAA Paper 2004-2129, 2004.

[6] Post, M. L., and Corke, T. C., "Separation Control on High Angle of Attack Airfoil Using Plasma Actuators," AIAA Paper 2003-1024, 2003.

[7] Post, M. L., and Corke, T. C., "Overview of Plasma Flow Control: Concepts, Optimization and Applications," AIAA Paper 2005-0563, 2005.

[8] Benard, N., Bonnet, J. P., Touchard, G., and Moreau, E., "Flow Control by Dielectric Barrier Discharge Actuators: Jet Mixing Enhancement," *AIAA Journal*, Vol. 46, No. 9, 2008, pp. 2293–2305. doi:10.2514/1.35404

[9] Kimmel, R. L., Hayes, J. R., Menart, J. A., and Shang, J., "Effect of Surface Plasma Discharges on Boundary Layers at Mach 5," AIAA Paper 2004-509, 2004.

[10] Raizer, Yu. P., *Gas Discharge Physics*, Springer, New York, 1991.

[11] Shin, J., Narayanaswamy, V., Raja, L. L., and Clemens, N. T., "Generation of Plasma Induced Flow Actuation by DC Glow-Like Discharge in a Supersonic Flow," AIAA Paper 2006-169, 2006.

[12] Shin, J., Narayanaswamy, V., Raja, L. L., and Clemens, N. T., "Characterization of a Direct-Current Glow Discharge Plasma Actuator in Low-Pressure Supersonic Flow," *AIAA Journal*, Vol. 45, No. 7, 2007, pp. 1596–1605. doi:10.2514/1.27197

[13] Leonov, S., Bityurin, V., Savelkin, K., and Yarantsev, D., "Effect of Electrical Discharge on Separation Processes and Shocks Position in Supersonic Airflow," AIAA Paper 2002-0355, 2002.

[14] Samimy, M., Adamovich, I., Webb, B., Kastner, J., Hileman, J., Keshav, S., and Palm, P., "Development and Characterization of Plasma Actuators for High Speed and Reynolds Number Jet Control," *Experiments in Fluids*, Vol. 37, No. 4, 2004, pp. 577-588. doi:10.1007/s00348-004-0854-7

[15] Samimy, M., Kim, J.-H., Kastner, J., Adamovich, I., and Utkin, Y., "Active Control of High Speed and High Reynolds Number Jets Using Plasma Actuators," *Journal of Fluid Mechanics*, Vol. 578, 2007, pp. 305–330. doi:10.1017/S0022112007004867

[16] Kalra, C., Zaidi, S., Alderman, B., Miles, R., and Murt, Y., "Magnetically Driven Surface Discharges for Shock-Wave Induced Boundary-Layer Separation Control," AIAA Paper 2007-222, 2007.

[17] Corke, T. C., Post, M. L., and Orlov, D. M., "Single Dielectric Barrier Discharge Plasma Enhance Aerodynamics: Physics, Modeling and Applications," *Experiments in Fluids*, Vol. 46, 2009, pp. 1–26. doi:10.1007/s00348-008-0582-5

[18] Kosinov, A., Maslov, A., and Shevelkov, S., "Experiments on the Stability of Supersonic Laminar Boundary Layers," *Journal of Fluid Mechanics*, Vol. 219, 1990, pp. 621–633. doi:10.1017/S0022112090003111

[19] Cybyk, B. Z., Grossman, K. R., and Wilerson, J. T., "Single Pulse Performance of the Sparkjet Flow Control Actuator," AIAA Paper 2003-57, 2003.

[20] Cybyk, B. Z., Simon, D. H., and Land, H. B., III, "Experimental Characterization of a Supersonic Flow Control Actuator," AIAA Paper 2006-478, 2006.

[21] Smy, P. R., Clements, R. M., Simeoni, D., and Topham, D. R., "Plasma Expulsion from the Plasma Jet Igniter," *Journal of Physics D: Applied Physics*, Vol. 15, 1982, pp. 2227–2239. doi:10.1088/0022-3727/15/11/015

[22] Smy, P. R., Santiago, J., and Way-Nee, D., "Momentum Imparted by Plasma Igniters to Surrounding Gas," *Journal of Physics D: Applied Physics*, Vol. 18, 1985, pp. 827–833. doi:10.1088/0022-3727/18/5/007

[23] Smith, M. F., "Observations of Supersonic Flat Plate Wakes," M.S. Thesis, Univ. of Texas at Austin, Austin, TX, 1995.

[24] McDaniel, J. C., and Graves, J., "Laser Induced Flourescence Visualization of Transverse Gaseous Injection in a Non-Reacting Supersonic Flow," *Journal of Propulsion and Power*, Vol. 4, 1988, pp. 591–597. doi:10.2514/3.23105

[25] Murugappan, S., Gutmark, E., and Carter, C., "Control of Penetration and Mixing of an Excited Supersonic Jet in Supersonic Crossflow," *Physics of Fluids*, Vol. 17, 2005, pp. 106101. doi:10.1063/1.2099027

[26] Kothnur, P. S., and Raja, L. L., "Two-Dimensional Simulation of a Direct-Current Microhollow Cathode Discharge," *Journal of Applied Physics*, Vol. 97, No. 4, 2005. doi:10.1063/1.1849816

[27] Shin, J., Narayanaswamy, V., Raja, L. L., and Clemens, N. T., "Characterization of a Direct-Current Glow Discharge Plasma Actuator in Low-Pressure Supersonic Flow," *AIAA Journal*, Vol. 45, No. 7, 2007, pp. 1596–1605. doi:10.2514/1.27197

[28] Utkin, Y., Keshav, S., Kim, J., Kastner., J., Adamovich, I., and Samimy, M., "Characterization of Localized Arc Filament Plasma Actuators Used for High-speed Flow Control," AIAA Paper 2007-787, 2007.

[29] Vincenti, W. G., and Kruger, C. H., "Introduction to Physical Gas Dynamics," Krieger, Malabar, FL, 1965.

[30] Engelhardt, A. G., Phelps, A. V., and Risk, C. G., "Determination of Momentum Transfer and Inelastic Collision Cross Sections for Electrons in Nitrogen Using Transport Coefficients," *Physical Review*, Vol. 135, No. 6A, 1964, pp. A1566–A1574. doi:10.1103/PhysRev.135.A1566

[31] Frost, L. S., and Phelps, A. V., "Rotational Excitation and Momentum Transfer Cross Section for Electrons in H_2 and N_2 from Transport Coefficients," *Physical Review*, Vol. 127, No. 5, 1962, pp. 1621–1633. doi:10.1103/PhysRev.127.1621

[32] Pitchford, L. C., Oneil, S. V., and Rumble, J. R., Jr., "Extended Boltzmann Analysis of Electron Swarm Experiments," *Physical Review A*, Vol. 23, No. 1, 1981, pp. 294–304. doi:10.1103/PhysRevA.23.294

[33] Pitchford, L. C., and Phelps, A. V., " Comparative Calculations of Electron-Swam Properties in N_2 at Moderate E/N Values," *Physical Review A*, Vol. 25, No. 1, 1982, pp. 540–554. doi:10.1103/PhysRevA.25.540

[34] Culick, F. E. C., Shen, P. I., and Griffin, W. S., "Acoustic Waves and Heating Due to Molecular Energy Transfer in an Electric Discharge CO Laser," *IEEE Journal of Quantum Electronics*, Vol. 12, No. 10, 1976, pp. 566–574. doi:10.1109/JQE.1976.1069042

[35] Smy, P. R., Clements, R. M., Dale, J. D., Simeoni, D., and Topham, D. R., "Efficiency and Erosion Characteristics of Plasma Jet Igniters," *Journal of Physics D: Applied Physics*, Vol. 16, 1983, pp. 783–791. doi:10.1088/0022-3727/16/5/011

[36] Anderson, J. D., "Modern Compressible Flow with Historic Perspective," McGraw–Hill, New York, 2002.

R. Lucht
Associate Editor